

Time-reversible high-order integrators for the nonlinear time-dependent Schrödinger equation: Application to local control theory

Julien Roulet and Jiří Vaníček^{a)}

Laboratory of theoretical physical chemistry, Institut des sciences et ingénieries Chimiques, Ecole Polytechnique Fédérale de Lausanne (EPFL), Lausanne, Switzerland

(Dated: 16 November 2021)

Local control theory is a technique for controlling the evolution of a molecular state with an electric field, whose amplitude is computed, using the current molecular state, in order to increase (or decrease) the expectation value of a chosen operator. Because the electric field depends on the molecular state, the time-dependent Schrödinger equation becomes nonlinear, which is often ignored in related studies that use a naïve implementation of the split-operator algorithm. To capture the nonlinearity, we present here high-order time-reversible integrators for the general time-dependent Schrödinger equation. These integrators are based on the symmetric compositions of the implicit midpoint method and, therefore, are norm-preserving, symmetric, time-reversible, and unconditionally stable. In contrast to split-operator algorithms, the proposed algorithms are also applicable to Hamiltonians nonseparable into a position- and momentum-dependent terms. The geometric properties of the integrators are proven analytically and demonstrated numerically on the local control of a two-dimensional model of retinal. Efficiency analysis shows that, for highly accurate calculations, the higher-order integrators are more efficient. For example, for an error of 10^{-9} , a 160000-fold speedup is observed when using the sixth-order method instead of the elementary explicit Euler method.

^{a)}Electronic mail: jiri.vanicek@epfl.ch

I. INTRODUCTION

By using ultrashort laser pulses, femtosecond chemistry^{1,2} made the real-time observation of the progress of chemical reactions possible. The possibility to shape the laser pulses, in turn, opened the way to quantum control, in which laser pulses are optimized in order to maximize the yield of the desired product of a chemical reaction. Several theoretical approaches to quantum control have been developed: The direct optimization of the pulse parameters is the most straightforward but it requires human input on the choice of the parameters which need to be optimized.³ Other methods such as pulse timing control,^{4,5} stimulated Raman adiabatic passage,⁶⁻⁹ and quantum optimal control theory^{4,10-14} (OCT) have been developed. In OCT, the control field is optimized using a variational principle combined with an iterative process, which requires forward and backward propagations in time—the method is said to be global in time. Despite its success, the repeated propagations of the system back and forth in time make the OCT computationally extremely expensive and, therefore, unfeasible for long simulations and systems with a large number of degrees of freedom.

Introduced by Kosloff *et al.*,¹³ local control theory (LCT) is another widely used approach to coherent control. LCT is computationally more affordable than the OCT because it does not require several propagations in time. In LCT, the pulse is instead computed on the fly, based on the instantaneous molecular state, in order to increase (or decrease) an expectation value of a specified operator. LCT has been successfully used to control various processes such as energy and population transfer,^{13,15-17} dissociation and association dynamics,¹⁸⁻²¹ direction of rotation in molecular rotors²², and electron transfer.²³

Controlling quantum systems using LCT changes the nature of the time-dependent Schrödinger equation. Because the time dependence of the pulse is determined exclusively by the molecular state, the time-dependent Schrödinger equation becomes autonomous but nonlinear. Unfortunately, in related studies, LCT was used without taking this nonlinearity into account. For example, a naïve adaptation of the second-order split-operator algorithm for linear Schrödinger equation²⁴ to the LCT was often used as a symmetric, time-reversible second-order method. In reality, because it neglects the nonlinear character of LCT, the naïve split-operator algorithm is only of first-order accuracy in the time step, and is neither symmetric nor time-reversible. As a consequence, the naïve algorithm is not suitable for

highly accurate calculations.

Recently, we presented high-order time-reversible geometric integrators for the nonadiabatic quantum dynamics driven by the linear time-dependent Schrödinger equation with both separable²⁵ and nonseparable²⁶ Hamiltonians. Here, we extend this work to the nonlinear case, and apply the high-order time-reversible algorithms proposed for the general nonlinear time-dependent Schrödinger equation to the special case of LCT. To address the slow convergence and nonconservation of geometric properties of the naïve split-operator algorithm for LCT, we propose integrators for solving nonlinear time-dependent Schrödinger equations which are highly accurate, efficient, stable regardless of the size of the time step, and preserve the geometric properties of the exact solution.

Nonlinear time-dependent Schrödinger equations contain, by definition, Hamiltonians that depend on the quantum state. Examples of situations, where such state-dependent Hamiltonians appear, include approximate equations for Bose-Einstein condensates,²⁷ for which the Hamiltonian depends on the probability density of the quantum state, the time-dependent variational principle, and some numerical methods such as the short-iterative Lanczos algorithm,^{28–30} where the effective Hamiltonian used for the propagation depends on the initial state.

The easiest method for solving the nonlinear time-dependent Schrödinger equation is the explicit Euler method. Unfortunately, this method is neither time-reversible nor symmetric; moreover, it is unstable, only of the first order of accuracy in the time step, and does not preserve the norm of the wavefunction.^{31,32} Composing a first-order method with its adjoint leads to symmetric second-order methods. The adjoint to the explicit Euler method is the implicit Euler method which is, again, neither symmetric nor time-reversible, first-order, and does not preserve the norm of the wavefunction. In contrast to its unstable explicit analogue, the implicit Euler method is asymptotically stable. Moreover, it is less straightforward to implement because, as its name suggests, it requires an implicit propagation. For a nonlinear time-dependent Schrödinger equation, this implicit propagation translates into solving a nonlinear system. For this, we use the Newton-Raphson method, in which iterations of the solution are obtained by solving a linear system—a task carried out by the generalized minimal residual method.^{33–35} By composing the explicit and implicit Euler methods we obtain the implicit midpoint method for the nonlinear time-dependent Schrödinger equation. This method is of second order of accuracy in the time step, time-reversible, symmetric,

norm-preserving, and stable regardless of the time step. Moreover, because it is symmetric, we can compose it with symmetric composition methods^{31,36–40} in order to obtain integrators of arbitrary even orders of accuracy which also conserve the geometric properties of the original method.

The remainder of the study is organized as follows: In Sec. II, we present the time-dependent Schrödinger equation within the electric dipole approximation, its associated exact evolution operator as well as its geometric properties. Next, we derive LCT and show how it results in a nonlinear time-dependent Schrödinger equation. In Sec. III, we first derive the exact evolution operator for time-dependent nonlinear Schrödinger equations, and then present the loss of geometric properties induced by using Euler methods. Following this, we present the recovery of these geometric properties by composition of the implicit and explicit Euler methods. Then, we describe a procedure to perform the implicit propagation and derive explicit expressions for the case of LCT. We also derive the naïve split-operator algorithm for the nonlinear Schrödinger equation and explain how it loses the geometric properties. Finally, we numerically verify in Sec. IV the convergence and geometric properties of the integrators by controlling, using LCT, either the population or energy transfer in a two-state two-dimensional model of retinal.⁴¹

II. NONLINEAR CHARACTER OF LOCAL CONTROL THEORY

A. Time-dependent Schrödinger equation within the electric dipole approximation

Quantum state $|\psi_t\rangle$ of a system interacting with a time-dependent electric field $\vec{E}(t)$ evolves according to the time-dependent Schrödinger equation

$$i\hbar \frac{d}{dt} |\psi_t\rangle = \hat{H}(t) |\psi_t\rangle \quad (1)$$

with a time-dependent Hamiltonian

$$\hat{H}(t) := \hat{H}_0 + \hat{V}_{\text{int}}(t), \quad (2)$$

equal to the sum of the Hamiltonian \hat{H}_0 of the system in the absence of the field and the interaction potential $\hat{V}_{\text{int}}(t)$. Within the long-wavelength and electric-dipole approximations,⁴²

the interaction potential is

$$\hat{V}_{\text{int}}(t) := -\vec{\mu}(\hat{q}) \cdot \vec{E}(t), \quad (3)$$

where $\vec{\mu}(\hat{q})$ denotes the electric-dipole operator of the system. Direct integration of Eq. (1) with initial condition $|\psi_{t_0}\rangle$ leads to the formal solution $|\psi_t\rangle = \hat{U}(t, t_0)|\psi_{t_0}\rangle$ with the exact evolution operator given by time-ordered exponential

$$\hat{U}(t, t_0) := \mathcal{T} \exp \left[-\frac{i}{\hbar} \int_{t_0}^t dt' \hat{H}(t') \right]. \quad (4)$$

This exact evolution operator has many important geometric properties: it is linear, unitary, symmetric, time-reversible, and stable.^{31,32,36,43} Because it is unitary, the evolution operator conserves the norm as well as the inner product and symplectic structure.³⁶ However, since the Hamiltonian is time-dependent, the Schrödinger equation (1) is a nonautonomous differential equation,³¹ and as a consequence, the exact evolution operator does not conserve the energy. For a more detailed presentation and discussion of the above properties, we refer the reader to Ref. 26.

B. Loss of linearity by LCT

Contrary to Eq. (3), the electric field used in LCT, called control field and denoted by $\vec{E}_{\text{LCT}}(t)$, is not known explicitly as a function of time. Instead, it is chosen “on the fly” according to the current state ψ_t of the system, in order to increase or decrease the expectation value $\langle \hat{O} \rangle_{\psi_t} := \langle \psi_t | \hat{O} | \psi_t \rangle$ of a particular operator \hat{O} in the state ψ_t . More precisely, the control field is computed so that the time derivative of the expectation value,

$$\begin{aligned} \frac{d\langle \hat{O} \rangle_{\psi_t}}{dt} &= \frac{i}{\hbar} \langle [\hat{H}(t), \hat{O}] \rangle_{\psi_t} \\ &= \frac{i}{\hbar} \left\{ \langle [\hat{H}_0, \hat{O}] \rangle_{\psi_t} + \langle [\hat{V}_{\text{int}}(t), \hat{O}] \rangle_{\psi_t} \right\} \\ &= \frac{i}{\hbar} \left\{ \langle [\hat{H}_0, \hat{O}] \rangle_{\psi_t} - \vec{E}_{\text{LCT}}(t) \cdot \langle [\hat{\vec{\mu}}, \hat{O}] \rangle_{\psi_t} \right\}, \end{aligned} \quad (5)$$

remains positive or negative at all times. If the operator \hat{O} commutes with the system’s Hamiltonian, this goal is achieved by using the field

$$\vec{E}_{\text{LCT}}(t) \equiv \vec{E}_{\text{LCT}}(\psi_t) := \pm \lambda i \langle [\hat{\vec{\mu}}, \hat{O}] \rangle_{\psi_t}^*, \quad (6)$$

where $\lambda > 0$ is a parameter which scales the intensity of the control field and the sign in Eq. (6) is chosen according to whether one wants to increase or decrease $\langle \hat{O} \rangle_{\psi_t}$. This claim

is proven by inserting the definition (6) of $\vec{E}_{\text{LCT}}(t)$ into the last line of Eq. (5), which yields

$$\frac{d\langle\hat{O}\rangle_{\psi_t}}{dt} = \frac{i}{\hbar}\langle[\hat{H}_0, \hat{O}]\rangle_{\psi_t} \pm \frac{\lambda}{\hbar}\|\langle[\hat{\mu}, \hat{O}]\rangle_{\psi_t}\|^2 \quad (7)$$

for the derivative of the expectation value. This equation implies that the rate of change of the expectation value we want to control is guaranteed to have a strictly positive or strictly negative range only if $[\hat{H}_0, \hat{O}] = 0$. A monotonic evolution of $\langle\hat{O}\rangle_{\psi_t}$ is, therefore, ensured only if $[\hat{H}_0, \hat{O}] = 0$, largely reducing the choice of operators whose expectation values we can control monotonically.

The left-hand side of Eq. (6) suggests that the control field can be either viewed as a function of time or a function of the molecular state [i.e., $\vec{E}_{\text{LCT}}(t) \equiv \vec{E}_{\text{LCT}}(\psi_t)$]. More precisely, the control field does not depend on time explicitly but only implicitly through the dependence on ψ_t . Therefore, the time-dependent Schrödinger equation changes from a nonautonomous linear to an autonomous nonlinear differential equation.³¹ By acknowledging this nonlinear character, the interaction potential shown in Eq. (3) becomes

$$\hat{V}_{\text{LCT}}(\psi_t) := -\hat{\mu} \cdot \vec{E}_{\text{LCT}}(\psi_t) \quad (8)$$

and Eq. (1) becomes an example of a *nonlinear time-dependent Schrödinger equation*

$$i\hbar\frac{d}{dt}|\psi_t\rangle = \hat{H}(\psi_t)|\psi_t\rangle \quad (9)$$

with the nonlinear Hamiltonian operator $\hat{H}(\psi) := \hat{H}_0 + \hat{V}_{\text{LCT}}(\psi)$ depending on the state of the system.

III. GEOMETRIC INTEGRATORS FOR THE NONLINEAR SCHRÖDINGER EQUATION

With initial condition $|\psi_{t_0}\rangle$, Eq. (9) has the formal solution $|\psi_t\rangle = \hat{U}(t, t_0; \psi)|\psi_{t_0}\rangle$ with the exact evolution operator given by

$$\hat{U}(t, t_0; \psi) := \mathcal{T} \exp \left[-\frac{i}{\hbar} \int_{t_0}^t dt' \hat{H}(\psi_{t'}) \right], \quad (10)$$

where the dependence of \hat{U} on ψ was added as an argument to emphasize the nonlinear character of Eq. (9).

This nonlinearity leads to the loss of some geometric properties, even if Eq. (9) is solved exactly. Indeed, since the Hamiltonian is nonlinear, the exact evolution operator is also nonlinear. As a consequence, it does not preserve the inner product⁴³ and it is neither symplectic nor unitary. Nevertheless, the exact evolution operator (10) remains symmetric, time-reversible, stable, and norm-preserving.

A. Loss of geometric properties by Euler methods

Numerical propagation methods for solving the nonlinear equation (9) obtain the state at time $t + \Delta t$ from the state at time t by using the relation

$$|\psi_{t+\Delta t}\rangle = \hat{U}_{\text{appr}}(t + \Delta t, t; \psi)|\psi_t\rangle, \quad (11)$$

where Δt denotes the numerical time step and $\hat{U}_{\text{appr}}(t + \Delta t, t; \psi)$ is an approximate nonlinear evolution operator depending on ψ .

The simplest methods, applicable to both separable and nonseparable and both linear and nonlinear Hamiltonian operators, are the *explicit* and *implicit* Euler^{32,36} methods which approximate the exact evolution operator as

$$\hat{U}_{\text{expl}}(t + \Delta t, t; \psi_t) := 1 - \frac{i}{\hbar} \hat{H}(\psi_t) \Delta t, \quad (12)$$

and

$$\hat{U}_{\text{impl}}(t + \Delta t, t; \psi_{t+\Delta t}) := \left[1 + \frac{i}{\hbar} \hat{H}(\psi_{t+\Delta t}) \Delta t \right]^{-1}, \quad (13)$$

respectively.

Both methods are only first-order in the time step and, therefore, very inefficient. Moreover, both Euler methods lead to the loss of some geometric properties of the exact evolution operator described by Eq. (10). As shown in Ref. 26, neither method is norm-preserving, symmetric, or time-reversible. Furthermore, the explicit Euler method is unstable and the implicit Euler method is asymptotically stable.

B. Recovery of geometric properties and increasing accuracy by composition

Composing the implicit and explicit Euler methods, in that order and with a time step $\Delta t/2$ for each, yields the *implicit midpoint* (or *Crank-Nicolson*) method

$$\begin{aligned} \hat{U}_{\text{mid}}(t + \Delta t, t; \psi_{t+\Delta t/2}) \\ &:= \hat{U}_{\text{expl}}(t + \Delta t, t + \Delta t/2; \psi_{t+\Delta t/2}) \\ &\quad \times \hat{U}_{\text{impl}}(t + \Delta t/2, t; \psi_{t+\Delta t/2}). \end{aligned} \quad (14)$$

This method is second-order in the time step, norm-preserving, symmetric, time-reversible, and stable regardless of the size of the time step.^{26,31}

Because it is symmetric, the midpoint method can be further composed using symmetric composition schemes^{26,31,36–40} in order to obtain integrators of arbitrary even order of accuracy in the time step. Indeed, every symmetric method \hat{U}_p of an even order p generates a method \hat{U}_{p+2} of order $p + 2$ if it is symmetrically composed as

$$\begin{aligned} \hat{U}_{p+2}(t + \Delta t, t) &:= \hat{U}_p(t + \gamma_M \Delta t, t + \gamma_{M-1} \Delta t) \\ &\quad \dots \hat{U}_p(t + \gamma_1 \Delta t, t), \end{aligned} \quad (15)$$

where M is the number of composition steps, $\gamma_1, \dots, \gamma_M$ are real composition coefficients which satisfy the relations $\sum_{n=1}^M \gamma_n = 1$, $\gamma_{M+1-n} = \gamma_n$, and a more-involved third condition³¹ guaranteeing the increase in the order of accuracy.

Note that exchanging the order of composition in Eq. (14) leads to the *trapezoidal* rule, which is also second-order, unitary, stable, symmetric, time-reversible, and can be composed to generate methods of arbitrary even orders.

C. Solving the implicit step

The implicit Euler method requires implicit propagation because its integrator [see Eq. (13)] depends on the result of the propagation, i.e., $\psi_{t+\Delta t}$. In the implicit Euler method, $\psi_{t+\Delta t}$ is obtained by solving the nonlinear system

$$\hat{U}_{\text{impl}}^{-1}(t + \Delta t, t; \psi_{t+\Delta t})|\psi_{t+\Delta t}\rangle = |\psi_t\rangle, \quad (16)$$

which can be written as $f(\psi_{t+\Delta t}) = 0$ with the nonlinear functional

$$\begin{aligned} f(\psi) &:= \hat{U}_{\text{impl}}^{-1}(\psi)\psi - \psi_t \\ &= \left[\hat{1} + \frac{i}{\hbar} \hat{H}(\psi) \Delta t \right] \psi - \psi_t. \end{aligned} \quad (17)$$

A nonlinear system $f(\psi) = 0$ can be solved with the iterative Newton-Raphson method, which computes, until convergence is obtained, the solution $\psi^{(k+1)}$ at iteration $k + 1$ from $\psi^{(k)}$ using the relation

$$\psi^{(k+1)} = \psi^{(k)} - \hat{J}^{-1}(\psi^{(k)})f(\psi^{(k)}), \quad (18)$$

where $\hat{J} := \frac{\delta}{\delta\psi} f(\psi)$ is the Jacobian of the nonlinear functional $f(\psi)$.

If the initial guess $\psi^{(0)}$ is close enough to the exact solution of the implicit propagation, the Newton-Raphson iteration (18) is a contraction mapping and by the fixed-point theorem is guaranteed to converge. We use as the initial guess the result of the explicit propagation of ψ_t with the explicit Euler method [Eq. (12)]. Note that this initial guess is sufficiently close to the implicit solution only if the time step is small. If the time step is too large, the difference between the explicit and implicit propagations becomes too large for the algorithm to converge and no solution can be obtained.

Equation (18) requires computing the inverse of the Jacobian which is an expensive task. It is preferable to avoid this inversion by computing each iteration as

$$\psi^{(k+1)} = \psi^{(k)} + \delta\psi^{(k)} \quad (19)$$

where $\delta\psi^{(k)}$ solves the linear system $\hat{J}(\psi^{(k)})\delta\psi^{(k)} = -f(\psi^{(k)})$. We solve this linear system by the generalized minimal residual method,^{33–35} an iterative method based on the Arnoldi process.^{44,45}

The procedure presented for solving the implicit propagation is applicable to any nonlinear system whose Jacobian is known analytically. Therefore, the integrators proposed in Secs. III A and III B can be employed for solving any nonlinear time-dependent Schrödinger equation of the form of Eq. (9), i.e., with a Hamiltonian $\hat{H}(\psi_t)$ depending on the state of the system.

D. Solving the implicit step in LCT

In the case of LCT,

$$\hat{U}_{\text{LCT,impl}}^{-1}(\psi) = \hat{1} + \frac{i}{\hbar} \Delta t \left[\hat{H}_0 + \hat{V}_{\text{LCT}}(\psi) \right],$$

and the Jacobian of the nonlinear functional (17) is given by

$$\begin{aligned} \hat{J}(\psi) &= \frac{\delta}{\delta\psi} \left[\hat{U}_{\text{LCT,impl}}^{-1}(\psi) \right] \psi + \hat{U}_{\text{LCT,impl}}^{-1}(\psi) \hat{1} \\ &= \frac{i}{\hbar} \Delta t \frac{\delta}{\delta\psi} \left[\hat{V}_{\text{LCT}}(\psi) \right] \psi + \hat{U}_{\text{LCT,impl}}^{-1}(\psi) \\ &= \frac{i}{\hbar} \Delta t \hat{V}_{\text{LCT}}(\psi) + \hat{1} + \frac{i}{\hbar} \Delta t \left[\hat{H}_0 + \hat{V}_{\text{LCT}}(\psi) \right] \\ &= \hat{1} + \frac{i}{\hbar} \Delta t \left[\hat{H}_0 + 2\hat{V}_{\text{LCT}}(\psi) \right]. \end{aligned} \tag{20}$$

To obtain the third row of Eq. (20), we used $\frac{\delta}{\delta\psi} \left[\hat{V}_{\text{LCT}}(\psi) \right] \psi = \hat{V}_{\text{LCT}}(\psi)$, where the generalized complex derivative⁴⁶ of the interaction potential is given by

$$\begin{aligned} \frac{\delta}{\delta\psi} \left[\hat{V}_{\text{LCT}}(\psi) \right] &= -\hat{\vec{\mu}} \cdot \frac{\delta}{\delta\psi} \left[\vec{E}_{\text{LCT}}(\psi) \right] \\ &= \mp \lambda i \hat{\vec{\mu}} \cdot \langle \psi | [\hat{\vec{\mu}}, \hat{O}] \rangle. \end{aligned} \tag{21}$$

E. Naïve application of the split-operator algorithm to the nonlinear Schrödinger equation

The algorithms that we described above apply not only to nonlinear but also to nonseparable Hamiltonians, i.e., to Hamiltonians \hat{H} which cannot be written as a sum $\hat{H} = T(\hat{p}) + V(\hat{q})$ of a momentum-dependent kinetic term and position-dependent potential term. If the time-dependent Schrödinger equation is linear and its Hamiltonian is separable, the midpoint method remains implicit, but the split-operator algorithms and their compositions yield explicit high-order integrators satisfying most geometric properties (except for the conservation of energy). In the case of LCT, if \hat{H}_0 is separable, so is the local control Hamiltonian, which can be written as $\hat{H}_{\text{LCT}}(\psi) = \hat{T} + \hat{V}_{\text{tot,LCT}}(\psi)$, where $\hat{V}_{\text{tot,LCT}}(\psi) := \hat{V}_0 + \hat{V}_{\text{LCT}}(\psi)$ is the sum of the system's and interaction potential energy operators. It is, therefore, tempting to use the split-operator algorithm, with the hope of obtaining an efficient explicit integrator.

More generally, let us assume that the Hamiltonian operator in the general nonlinear Schrödinger equation (9) can be separated as

$$\hat{H}(\psi) = T(\hat{p}) + V_{\text{tot}}(\hat{q}, \psi).$$

The approximate evolution operator is given by

$$\hat{U}_{\text{TV}}(t + \Delta t; t, \psi_t) := e^{-\frac{i}{\hbar}\hat{T}\Delta t} e^{-\frac{i}{\hbar}\hat{V}_{\text{tot}}(\psi_t)\Delta t} \quad (22)$$

in the *TV* split-operator algorithm and by

$$\hat{U}_{\text{VT}}(t + \Delta t; t, \psi_{t+\Delta t}) := e^{-\frac{i}{\hbar}\hat{V}_{\text{tot}}(\psi_{t+\Delta t})\Delta t} e^{-\frac{i}{\hbar}\hat{T}\Delta t} \quad (23)$$

in the *VT* split-operator algorithm. These integrators are norm-preserving but only first-order. Moreover, they do not preserve the inner product and are neither symmetric nor time-reversible. From their definitions (22) and (23), it follows immediately that the TV and VT algorithms are adjoints²⁵ of each other and require, respectively, explicit and implicit propagations. In analogy to the implicit midpoint algorithm from Sec. III B, a second-order method is obtained by composing the two adjoint methods to obtain the *TVT* split-operator algorithm

$$\begin{aligned} \hat{U}_{\text{TVT}}(t + \Delta t; t, \psi_{t+\Delta t/2}) \\ := \hat{U}_{\text{TV}}(t + \Delta t; t + \Delta t/2, \psi_{t+\Delta t/2}) \\ \times \hat{U}_{\text{VT}}(t + \Delta t/2; t, \psi_{t+\Delta t/2}), \end{aligned} \quad (24)$$

or the *VTV* split-operator algorithm if the order of composition is reversed. Although neither second-order method preserves the inner product, both are norm-preserving, symmetric, and time-reversible. However, these geometric properties are only acquired if the implicit part, i.e., the propagation with the VT algorithm (24) is performed exactly. This requires solving a nonlinear system, which can be performed using the Newton-Raphson method, as described in Sec. III C. This, however, implies abandoning the explicit nature of the split-operator algorithm, which is one of its main advantages over implicit methods for solving linear Schrödinger equations.

In many works, the nonlinear character of Eq. (9) is often ignored and an inappropriate state is used for performing both steps in Eq. (24). For example, instead of $\psi_{t+\Delta t}$, the state

$\psi_{\hat{T}, t+\Delta t/2} := e^{-\frac{i}{\hbar}\hat{T}\Delta t/2}\psi_t$ obtained after the kinetic propagation is often used, which yields the *naïve TVT* split-operator algorithm

$$\begin{aligned} \hat{U}_{\text{naïve TVT}}(t + \Delta t; t, \psi_{\hat{T}, t+\Delta t/2}) \\ := \hat{U}_{\text{TV}}(t + \Delta t; t + \Delta t/2, \psi_{\hat{T}, t+\Delta t/2}) \\ \times \hat{U}_{\text{VT}}(t + \Delta t/2; t, \psi_{\hat{T}, t+\Delta t/2}). \end{aligned} \quad (25)$$

Because this naïve explicit integrator depends on $\psi_{\hat{T}, t+\Delta t/2}$ instead of $\psi_{t+\Delta t/2}$, it is neither symmetric nor time-reversible and achieves only first-order accuracy in the time step. While it still does not preserve the inner product (because it is nonlinear), the naïve algorithm is norm-preserving and, therefore, stable.

IV. NUMERICAL EXAMPLES

We tested the general integrators for the nonlinear Schrödinger equation, presented in Sec. II, by using them for the local control of a two-dimensional two-state diabatic model of retinal taken from Ref. 41. The model describes the cis-trans photo-induced isomerization of retinal—an ultrafast reaction mediated by a conical intersection and the first event occurring in the biological process of vision. The two vibrational modes of the model are the reaction coordinate ϕ , an angle describing the torsional motion of the retinal molecule, and a vibronically active coupling mode q_c . In the diabatic representation, the Hamiltonian of the system in the absence of the field,

$$\hat{\mathbf{H}}_0 = \hat{T}\mathbf{1} + \begin{pmatrix} \hat{V}_{11}(q_c, \phi) & \hat{V}_{12}(q_c) \\ \hat{V}_{21}(q_c) & \hat{V}_{22}(q_c, \phi) \end{pmatrix}, \quad (26)$$

is separable into a sum of the kinetic energy operator

$$\hat{T} = -\frac{1}{2}\omega\frac{\partial^2}{\partial q_c^2} - \frac{1}{2}m^{-1}\frac{\partial^2}{\partial \phi^2} \quad (27)$$

and potential energy operator with components

$$\hat{V}_{11}(q_c, \phi) = \frac{1}{2}\omega q_c^2 + \frac{1}{2}W_1 [1 - \cos(\phi)], \quad (28)$$

$$\hat{V}_{22}(q_c, \phi) = \frac{1}{2}\omega q_c^2 + \kappa_2 q_c + E_2 - \frac{1}{2}W_2 [1 - \cos(\phi)], \quad (29)$$

$$\hat{V}_{12}(q_c) = \hat{V}_{21}(q_c) = \lambda q_c. \quad (30)$$

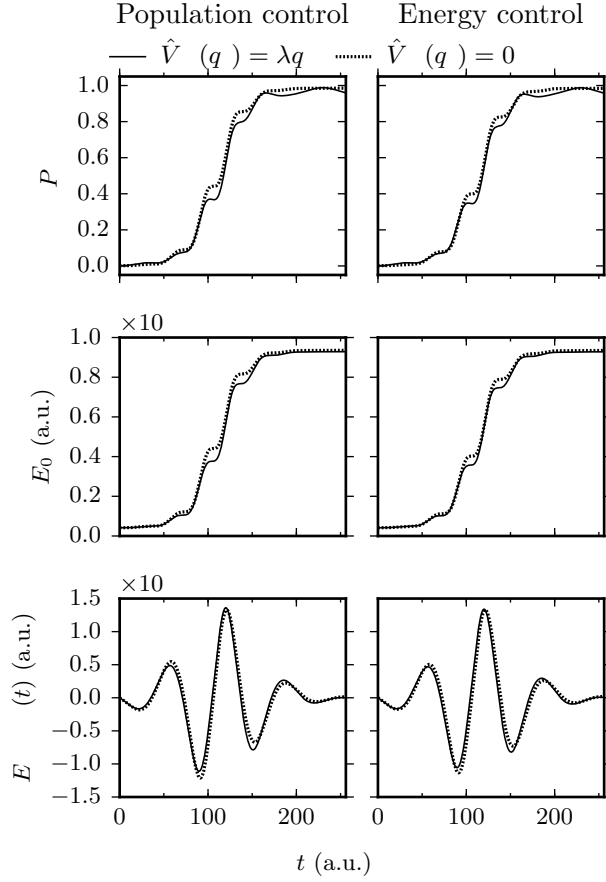


FIG. 1. Local control calculations whose goal is increasing either the population $P_2 := \langle \mathbf{P}_2 \rangle_{\psi_t}$ of the excited state (left panels, $\lambda = 1.430 \times 10^{-2}$) or the total molecular energy $E_0 := \langle \hat{\mathbf{H}}_0 \rangle_{\psi_t}$ (right panels, $\lambda = 1.534 \times 10^{-1}$). As expected, the local control theory applied to these closely related objectives yields very similar results. Top: Excited state population. Middle: Molecular energy. Bottom: Pulse obtained by local control theory. Nonadiabatic couplings give rise to a non-monotonic time evolution of the population [solid lines, the couplings are given by Eq. (30)]. Compare this with the monotonic increase of the population in the absence of nonadiabatic couplings [dotted lines, the couplings are given by $\hat{V}_{12}(q_c) = \hat{V}_{21}(q_c) = 0$].

Here (all parameters are in eV units), $\omega = 0.19$ is the vibrational frequency of the coupling mode, $m^{-1} = 4.84 \cdot 10^{-4}$ is the inverse mass of the reaction coordinate, $W_1 = 3.6$ and $W_2 = 1.09$ determine the depth of the well in the reaction coordinate for the ground and excited electronic states, respectively, $\kappa_2 = 0.1$ is the gradient of the linear perturbation in the excited electronic state, $E_2 = 2.48$ determines the maximum of the excited electronic state in the reaction coordinate, and $\lambda = 0.19$ is the gradient of the linear coupling between

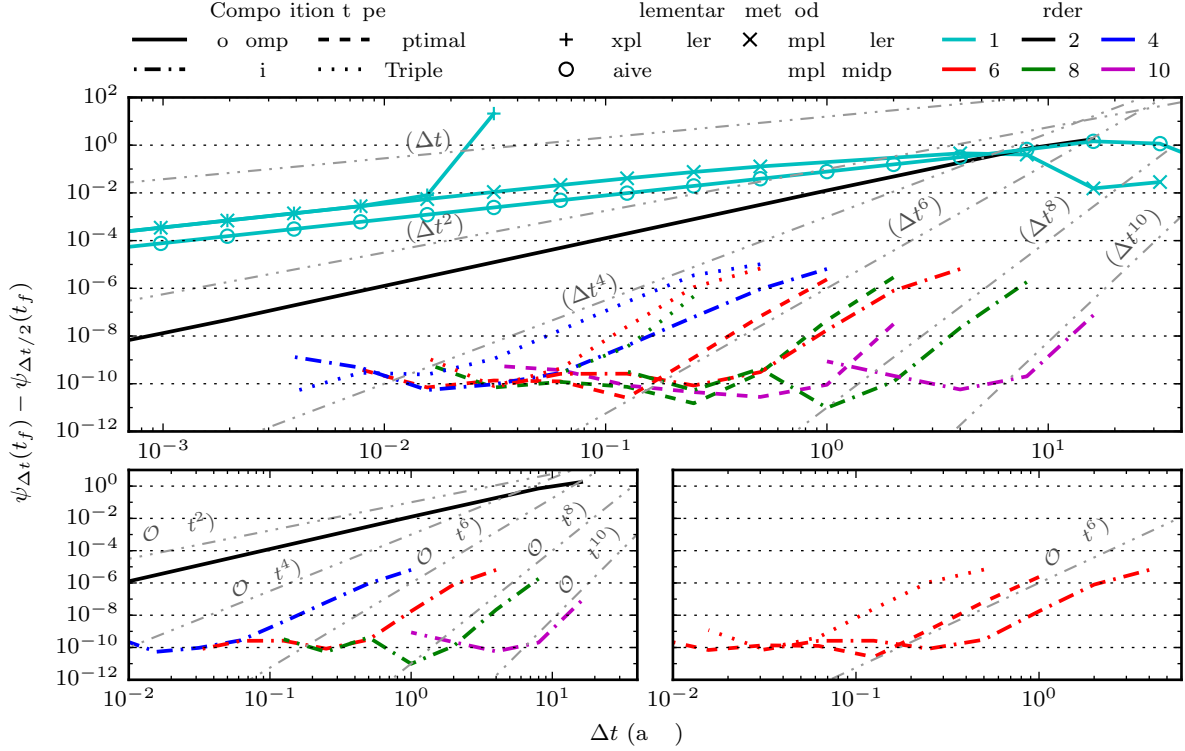


FIG. 2. Convergence of the molecular wavefunction at the final time t_f achieved by the local control of population in the presence of nonadiabatic couplings. Top: All studied methods, i.e., explicit and implicit Euler methods, naïve TVT split-operator algorithm, implicit midpoint method and its symmetric compositions. Bottom-left: Methods obtained with the Suzuki composition scheme. Bottom-right: Sixth-order methods obtained with different composition schemes.

the two electronic states. (Note that the **bold** face denotes electronic operators expressed as $S \times S$ matrices in the basis of S electronic states and that the hat $\hat{\cdot}$ denotes nuclear operators acting on the Hilbert space of nuclear wavefunctions, i.e., square-integrable functions of D continuous dimensions.) In the simulations, the reaction and coupling coordinates are represented on regular grids consisting, respectively, of 256 points between $\phi = -\pi/2$ a.u. and $\phi = 3\pi/2$ a.u. and 64 points between $q_c = -4.25$ a.u. and $q_c = 4.25$ a.u. We also assume constant and unit transition-dipole elements in the y -direction only, and that all diagonal elements of the electric dipole operator are zero. The calculations presented below aim to simulate the photo-excitation step of the photo-isomerization of the retinal molecule. We therefore used as initial state ψ_0 the ground vibrational state of the harmonic fit of the ground electronic state [i.e., a two-dimensional Gaussian wavepacket with $q_0 = (0, 0)$, $p_0 =$

(0, 0), and $\sigma_0 = (0.128, 1)$ a.u.] with initial populations $P_1(0) = 0.999$ and $P_2(0) = 0.001$ of the ground and excited electronic states, respectively. The tiny initial seed population on the excited state is essential for the control because it ensures that Eq. (6) does not stay zero at all times.

Two ways of populating the excited state based on LCT were investigated: the former used as the target observable the population of the excited state described by the projection operator onto the excited state (i.e., $\hat{\mathbf{O}} = \mathbf{P}_2\hat{1} = \mathbf{P}_2$), while the latter employed as the target observable the molecular energy described by the unperturbed molecular Hamiltonian as the control operator (i.e., $\hat{\mathbf{O}} = \hat{\mathbf{H}}_0$). The control calculations were performed by solving the nonlinear time-dependent Schrödinger equation (9) with the implicit midpoint algorithm combined with the dynamic Fourier method^{24,47–49} for a total time $t_f = 256$ a.u. with a time step $\Delta t = 2^{-3}$ a.u. In addition, intensity parameters $\lambda = 1.430 \times 10^{-2}$ and $\lambda = 1.534 \times 10^{-1}$ were used for the control of excited-state population $P_2(t) = \langle \mathbf{P}_2 \rangle_{\psi_t}$ and molecular energy $E_0(t) = \langle \hat{\mathbf{H}}_0 \rangle_{\psi_t}$, respectively. These parameters were chosen so that the electric fields of the obtained control pulses were similar during the first period.

Populations, expectation value of energy, and obtained control pulses for the control of excited-state population (left column) and molecular energy (right column) are shown in Fig. 1. In the figure, the results obtained in the presence and in the absence of nonadiabatic couplings are also compared for each target. The population and energy control schemes result in similar population dynamics and in both schemes, the population of the excited state reaches 0.95 at time t_f . As expected, when controlling the excited-state population ($\langle \mathbf{P}_2 \rangle_{\psi_t}$) in the presence of nonadiabatic couplings, the evolution of the population is not monotonic because the control operator does not commute with the molecular Hamiltonian (i.e., $[\mathbf{P}_2, \hat{\mathbf{H}}_0] \neq 0$). In contrast, when controlling the molecular energy ($\langle \hat{\mathbf{H}}_0 \rangle_{\psi_t}$), its time evolution is always monotonic because the molecular Hamiltonian commutes with itself, whether or not the nonadiabatic couplings are included. Because increasing the population of the excited state has almost the same effect as increasing the molecular energy, very similar dynamics and control pulses are obtained. Yet, the energy and population controls do not always yield similar results. In the retinal model, when performing energy control, no vibrational energy is pumped into the system because the diagonal terms of the electric-dipole moment operator are, by construction, all zero (hence $\langle [\hat{\boldsymbol{\mu}}, \hat{\mathbf{T}}] \rangle_{\psi_t} = 0$). Consequently, only potential energy is added to the system, and the corresponding control pulse is similar

to the one obtained from the population control.

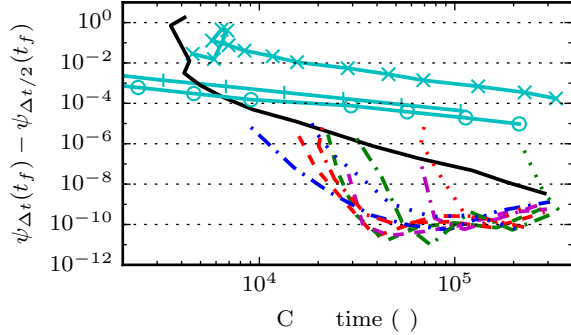


FIG. 3. Efficiency of the integrators used for the local population control of retinal in the presence of nonadiabatic couplings. Efficiency is measured by plotting the convergence error as a function of the computational (CPU) cost. Simulations were performed using both Euler methods, the naïve TVT split-operator algorithm as well as the implicit midpoint method and its symmetric compositions. Line labels are the same as in Fig. 2.

To verify the orders of convergence predicted in Sec. III B, we performed convergence analysis of control simulations using various integrators. Simulations with each integrator were repeated several times with different time steps and the resulting wavefunctions at the final time t_f were compared. As a measure of the convergence error, we used the L_2 -norm $\|\psi_{\Delta t}(t_f) - \psi_{\Delta t/2}(t_f)\|$, where $\psi_{\Delta t}(t_f)$ is the final wavefunction obtained after propagation with time step Δt . Figure 2 displays the convergence behavior of both Euler methods, the naïve TVT split-operator algorithm, and the proposed implicit midpoint method as well as its symmetric compositions, when controlling the excited state population. Notice that all of the integrators have their predicted orders of convergence. The naïve TVT split-operator algorithm is, for the reasons mentioned in Sec. III E, only first-order and not second-order as one might naïvely expect. For the convergence of other simulations, we refer the reader to Figs. S1-S3 of the supporting information. Together, these results imply that both population and energy control follow the correct order of convergence and that the presence of nonadiabatic couplings does not prevent the integrators from converging with their expected order.

Because the higher-order methods require more work to perform each step, a higher order of convergence may not guarantee higher efficiency. Therefore, we evaluated the efficiency

of each method directly by measuring the computational cost needed to reach a prescribed convergence error. Figure 3 shows the convergence error as a function of the central processing unit (CPU) time and confirms that, except for very crude calculations, higher-order integrators are more efficient than any of the first- and second-order methods. For example, to reach errors below a rather high threshold of 2×10^{-5} , the fourth-order integrator obtained with the Suzuki composition scheme is *already* more efficient than any of the first- or second-order algorithms. The efficiency gain becomes more important when highly accurate results are desired. Indeed, for an error of 10^{-9} , the sixth-order optimal method is approximately 160000 times faster than the first-order explicit Euler method and 17 times faster than the second-order implicit midpoint method. Whereas the naïve TVT split-operator algorithm is slightly more efficient than the explicit Euler method, high accuracy is hard to achieve with this integrator. Notice that the cost of implicit methods is not a monotonous function of the error because the Newton-Raphson method needs more iterations to converge for larger than smaller time steps. Indeed, for time steps (or errors) larger than a critical value, the CPU time might in fact increase with further increasing time step (or error). The efficiency plots of other control simulations (see Fig. S4-S6 of the supporting information) confirm that the increase in efficiency persists regardless of the control target (energy or population) and presence or absence of nonadiabatic couplings.

We also checked the conservation of geometric properties by the proposed integrators. Exact conservation of the norm is demonstrated in the left panel of Fig. 4 for both the naïve TVT split-operator algorithm and the implicit midpoint method as well as all of its symmetric compositions. In contrast, neither Euler method conserves the norm. As expected from a nonlinear differential equation, the inner product is not conserved (see the center panel of Fig. 4). Finally, the right panel of Fig. 4 shows that neither the naïve TVT split-operator algorithm nor any Euler method is time-reversible, whereas the implicit midpoint method and all of its symmetric compositions are exactly time-reversible. Note that in Fig. 4, simulations performed with the implicit midpoint method and its compositions become less norm-preserving and less time-reversible as the time step decreases. This is a consequence of an accumulation of numerical errors at each step of the propagation. Concerning other simulations, almost identical results are observed (see Figs. S7-S9 of the supporting information), which confirms that neither the chosen objective nor the nonadiabatic couplings influence the geometric properties of the integrators.

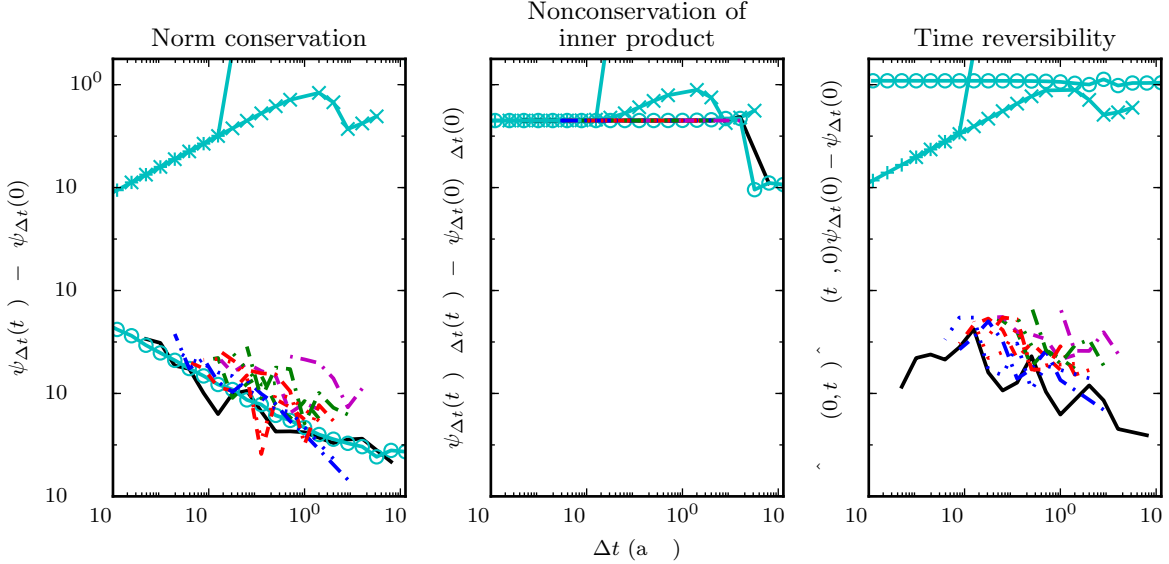


FIG. 4. Conservation of norm (left), inner product (center) and time reversibility (right) of the integrators for the local control of population in the presence of nonadiabatic couplings. $\theta(0)$ is $\psi(0)$ displaced along the reaction coordinate, i.e., a Gaussian wavepacket with parameters $q_0 = (0.1, 0)$, $p_0 = (0, 0)$, and $\sigma_0 = (0.128, 0)$ a.u. Time reversibility is measured as the distance between the initial state ψ_0 and a state $\hat{U}_{\text{LCT}}(0, t_f)\hat{U}_{\text{LCT}}(t_f, 0)\psi(0)$, obtained by propagating $\psi(0)$ first forward in time for time t_f and then backward in time for time t_f . Line labels are the same as in Fig. 2.

V. CONCLUSION

We presented high-order time-reversible integrators for the nonlinear time-dependent Schrödinger equation and demonstrated their efficiency and geometric properties on the problem of local control of quantum systems. The basic time-reversible integrator is an adaptation of the implicit midpoint method to the nonlinear Schrödinger equation and is obtained by composing the explicit and implicit Euler methods. It is norm-preserving, symmetric, time-reversible, unconditionally stable, and of second order of accuracy in the time step.

Because it is symmetric, the implicit midpoint method can be composed using symmetric composition methods to obtain integrators of an arbitrary even order of accuracy. These higher-order integrators conserve all of the properties of the original method.

In contrast, the naïve TVT split-operator algorithm is an erroneous adaptation of the

standard second-order TVT split-operator algorithm to the nonlinear Schrödinger equation. Because this integrator does not account for the nonlinearity, it is only of first-order accuracy in the time step and loses time reversibility while still preserving the norm.

The convergence behavior and geometric properties of the integrators were justified analytically and demonstrated numerically on a two-dimensional model of retinal where a photoexcitation process was simulated by controlling either the population of the excited state or the molecular energy. Comparison of numerical efficiencies of the different integrators showed that the higher-order integrators are more efficient, when high accuracy is required, compared to the first- and second-order integrators. Indeed, these higher-order integrators sped up the calculations by several orders of magnitude, while remaining time-reversible, symmetric and norm-conserving. For example, for an error lower than 10^{-9} , the sixth-order integrator obtained with the optimal composition method reduces the CPU time of the calculation by a factor of 160000 compared to the explicit Euler method and by a factor of 17 compared to the implicit midpoint method. Moreover, we found that the control objective and the presence or absence of nonadiabatic couplings have little influence on the convergence, efficiency, and geometric properties of the integrators.

Although we applied the algorithms only to the special case of LCT, they should be useful for any nonlinear time-dependent Schrödinger equation if high accuracy and time reversibility of the solution are desired.

The data that support the findings of this study are available from the corresponding author upon reasonable request.

ACKNOWLEDGEMENTS

The authors thank Seonghoon Choi for useful discussions and acknowledge the financial support from the Swiss National Science Foundation within the National Center of Competence in Research “Molecular Ultrafast Science and Technology” (MUST).

REFERENCES

¹A. H. Zewail, *J. Phys. Chem. A* **104**, 5660 (2000).

²A. Mokhtari, P. Cong, J. L. Herek, and A. H. Zewail, *Nature* **348**, 225 (1990).

- ³W. Jakubetz, B. Just, J. Manz, and H. J. Schreier, *J. Chem. Phys.* **94**, 2294 (1990).
- ⁴D. J. Tannor and S. A. Rice, *J. Chem. Phys.* **83**, 5013 (1985).
- ⁵D. J. Tannor, R. Kosloff, and S. A. Rice, *J. Chem. Phys.* **85**, 5805 (1986).
- ⁶K. Bergmann, H. Theuer, and B. W. Shore, *Rev. Mod. Phys.* **70**, 1003 (1998).
- ⁷N. V. Vitanov, T. Halfmann, B. W. Shore, and K. Bergmann, *Annu. Rev. Phys. Chem.* **52**, 763 (2001).
- ⁸G. W. Coulston and K. Bergmann, *J. Chem. Phys.* **96**, 3467 (1992).
- ⁹U. Gaubatz, P. Rudecki, S. Schiemann, and K. Bergmann, *J. Chem. Phys.* **92**, 5363 (1990).
- ¹⁰A. P. Peirce, M. A. Dahleh, and H. Rabitz, *Phys. Rev. A* **37**, 4950 (1988).
- ¹¹W. Zhu, J. Botina, and H. Rabitz, *J. Chem. Phys.* **108**, 1953 (1998).
- ¹²W. Zhu and H. Rabitz, *J. Chem. Phys.* **109**, 385 (1998).
- ¹³R. Kosloff, S. A. Rice, P. Gaspard, S. Tersigni, and D. J. Tannor, *Chem. Phys.* **139**, 201 (1989).
- ¹⁴J. Werschnik and E. K. U. Gross, *J. Phys. B* **40**, R175 (2007).
- ¹⁵R. Kosloff, A. D. Hammerich, and D. Tannor, *Phys. Rev. Lett.* **69**, 2172 (1992).
- ¹⁶P. Marquetand, S. Grfe, D. Scheidel, and V. Engel, *J. Chem. Phys.* **124**, 054325 (2006).
- ¹⁷V. Engel, C. Meier, and D. J. Tannor, *Adv. Chem. Phys.* **141** (2009).
- ¹⁸P. Marquetand and V. Engel, *Chem. Phys. Lett.* **426**, 263 (2006).
- ¹⁹P. Marquetand and V. Engel, *J. Chem. Phys.* **127**, 084115 (2007).
- ²⁰L. Bomble, A. Chenel, C. Meier, and M. Desouter-Lecomte, *J. Chem. Phys.* **134**, 204112 (2011).
- ²¹S. Vranckx, J. Loreau, N. Vaeck, C. Meier, and M. Desouter-Lecomte, *J. Chem. Phys.* **143**, 164309 (2015).
- ²²M. Yamaki, K. Hoki, Y. Ohtsuki, H. Kono, and Y. Fujimura, *J. Am. Chem. Soc.* **127**, 7300 (2005).
- ²³P. Vindel-Zandbergen, C. Meier, and I. R. Sola, *Chem. Phys. Charge Carrier Dynamics at the Nanoscale*, **478**, 97 (2016).
- ²⁴M. D. Feit, J. A. Fleck, Jr., and A. Steiger, *J. Comp. Phys.* **47**, 412 (1982).
- ²⁵J. Roulet, S. Choi, and J. Vaníček, *J. Chem. Phys.* **150**, 204113 (2019).
- ²⁶S. Choi and J. Vaníček, *J. Chem. Phys.* **150**, 204112 (2019).
- ²⁷F. Dalfovo, S. Giorgini, L. P. Pitaevskii, and S. Stringari, *Rev. Mod. Phys.* **71**, 463 (1999).

- ²⁸C. Lanczos, J. Res. Nat. Bur. Stand. **45**, 255 (1950).
- ²⁹C. Leforestier, R. H. Bisseling, C. Cerjan, M. D. Feit, R. Friesner, A. Guldberg, A. Hammerich, G. Jolicard, W. Karrlein, H.-D. Meyer, N. Lipkin, O. Roncero, and R. Kosloff, J. Comp. Phys. **94**, 59 (1991).
- ³⁰T. J. Park and J. C. Light, J. Chem. Phys. **85**, 5870 (1986).
- ³¹E. Hairer, C. Lubich, and G. Wanner, *Geometric Numerical Integration: Structure-Preserving Algorithms for Ordinary Differential Equations* (Springer Berlin Heidelberg New York, 2006).
- ³²B. Leimkuhler and S. Reich, *Simulating Hamiltonian Dynamics* (Cambridge University Press, 2004).
- ³³W. H. Press, S. A. Teukolsky, W. T. Vetterling, and B. P. Flannery, *Numerical recipes in C* (Cambridge University Press, Cambridge, UK, 1992).
- ³⁴Y. Saad and M. H. Schultz, SIAM J. Sci. Comp. **7**, 856 (1986).
- ³⁵Y. Saad, *Iterative Methods for Sparse Linear Systems*, 2nd ed. (SIAM, 2003).
- ³⁶C. Lubich, *From Quantum to Classical Molecular Dynamics: Reduced Models and Numerical Analysis*, 12th ed. (European Mathematical Society, Zürich, 2008).
- ³⁷H. Yoshida, Phys. Lett. A **150**, 262 (1990).
- ³⁸M. Suzuki, Phys. Lett. A **146**, 319 (1990).
- ³⁹W. Kahan and R.-C. Li, Math. Comput. **66**, 1089 (1997).
- ⁴⁰M. Sofroniou and G. Spaletta, Optim. Method Softw. **20**, 597 (2005).
- ⁴¹S. Hahn and G. Stock, J. Phys. Chem. B **104**, 1146 (2000).
- ⁴²G. C. Schatz and M. A. Ratner, *Quantum Mechanics in Chemistry* (Dover Publications, 2002).
- ⁴³P. R. Halmos, *Finite dimensional vector spaces* (Princeton University Press, 1942).
- ⁴⁴W. E. Arnoldi, Quart. Appl. Math **9**, 17 (1951).
- ⁴⁵Y. Saad, Linear Algebra Appl. **34**, 269 (1980).
- ⁴⁶K. B. Petersen and M. S. Pedersen, “The matrix cookbook,” (2012).
- ⁴⁷D. J. Tannor, *Introduction to Quantum Mechanics: A Time-Dependent Perspective* (University Science Books, Sausalito, 2007).
- ⁴⁸D. Kosloff and R. Kosloff, J. Comp. Phys. **52**, 35 (1983).
- ⁴⁹R. Kosloff and D. Kosloff, J. Chem. Phys. **79**, 1823 (1983).

Supporting information: A time-reversible integrator for local control theory

Julien Roulet and Jiří Vaníček^{a)}

*Laboratory of theoretical physical chemistry, Institut des sciences et
ingénieries Chimiques, Ecole Polytechnique Fédérale de Lausanne (EPFL),
and*

Lausanne, Switzerland

(Dated: 16 November 2021)

^{a)}Electronic mail: jiri.vanicek@epfl.ch

I. CONVERGENCE, EFFICIENCY AND GEOMETRIC PROPERTIES OF THE INTEGRATORS FOR THE OTHER SIMULATIONS

We present here the results obtained when controlling the population (in the absence of nonadiabatic couplings) as well as the energy (in the presence and in the absence of nonadiabatic couplings).

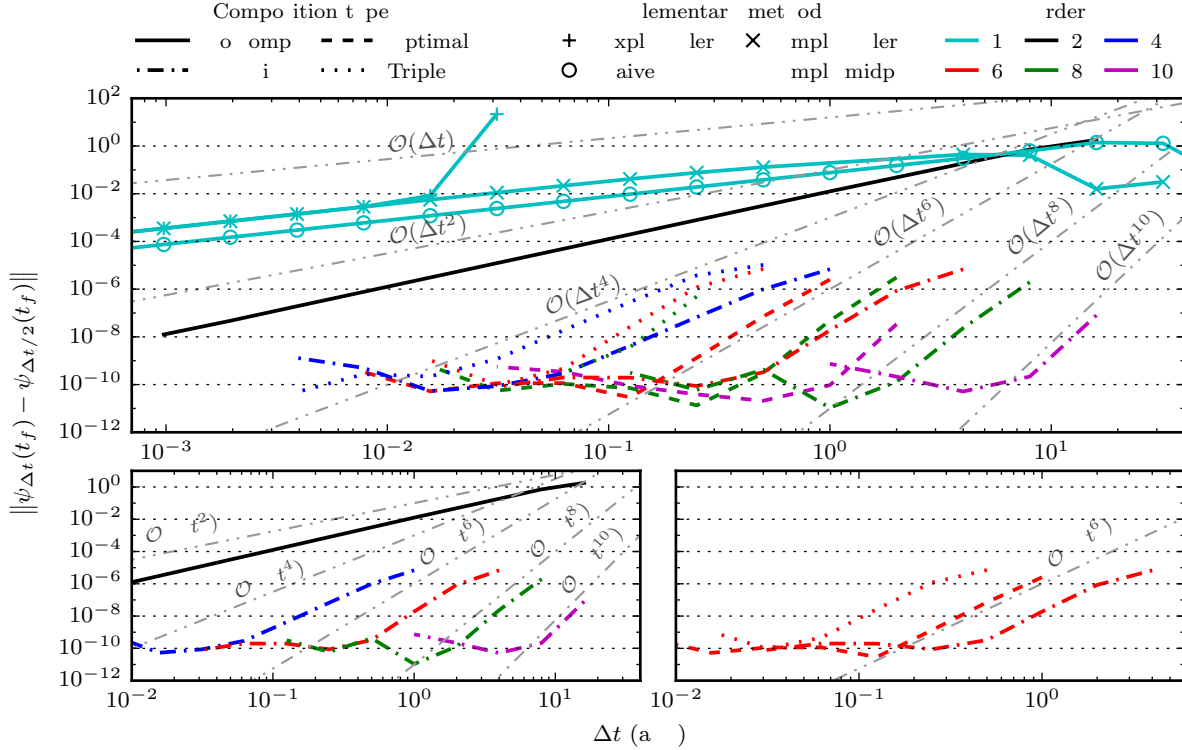


FIG. S1. Convergence of the molecular wavefunction at the final time t_f achieved by the local control of population in the absence of nonadiabatic couplings. Top: All studied methods, i.e., explicit and implicit Euler methods, naïve TVT split-operator algorithm, implicit midpoint method and its symmetric compositions. Bottom-left: Methods obtained with the Suzuki composition scheme. Bottom-right: Sixth-order methods obtained with different composition schemes.

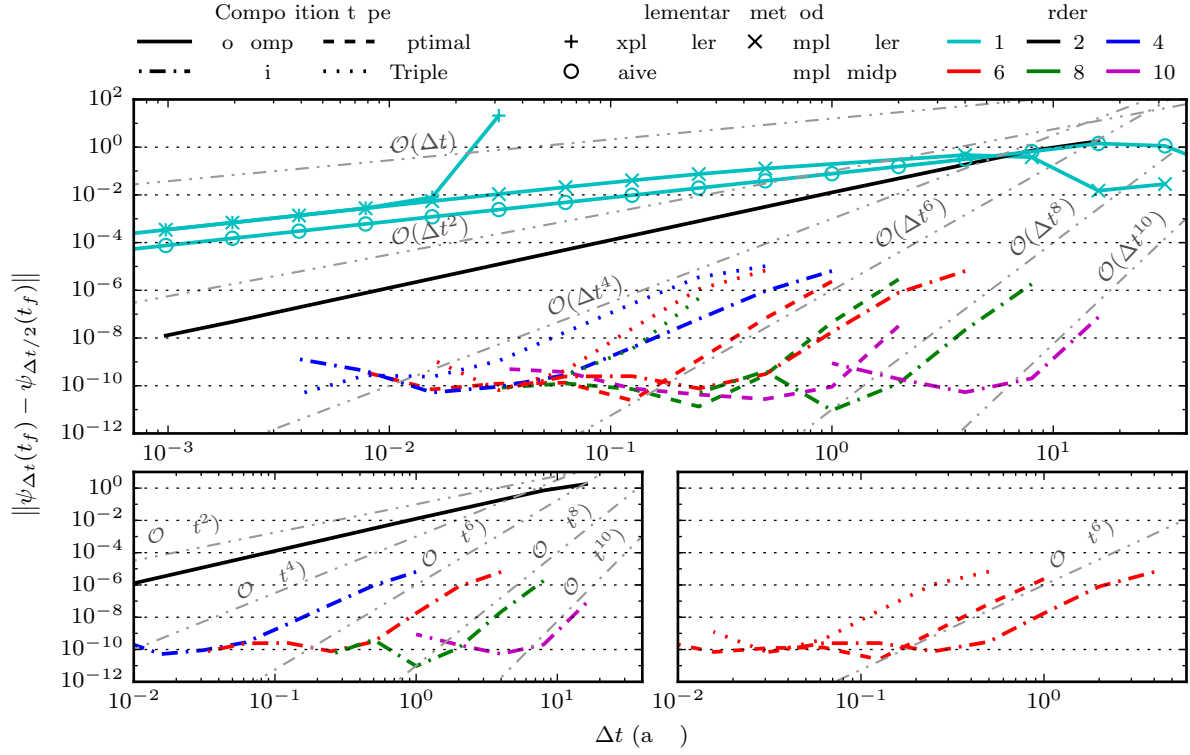


FIG. S2. Same as Fig. S1, but for energy control with nonadiabatic couplings.

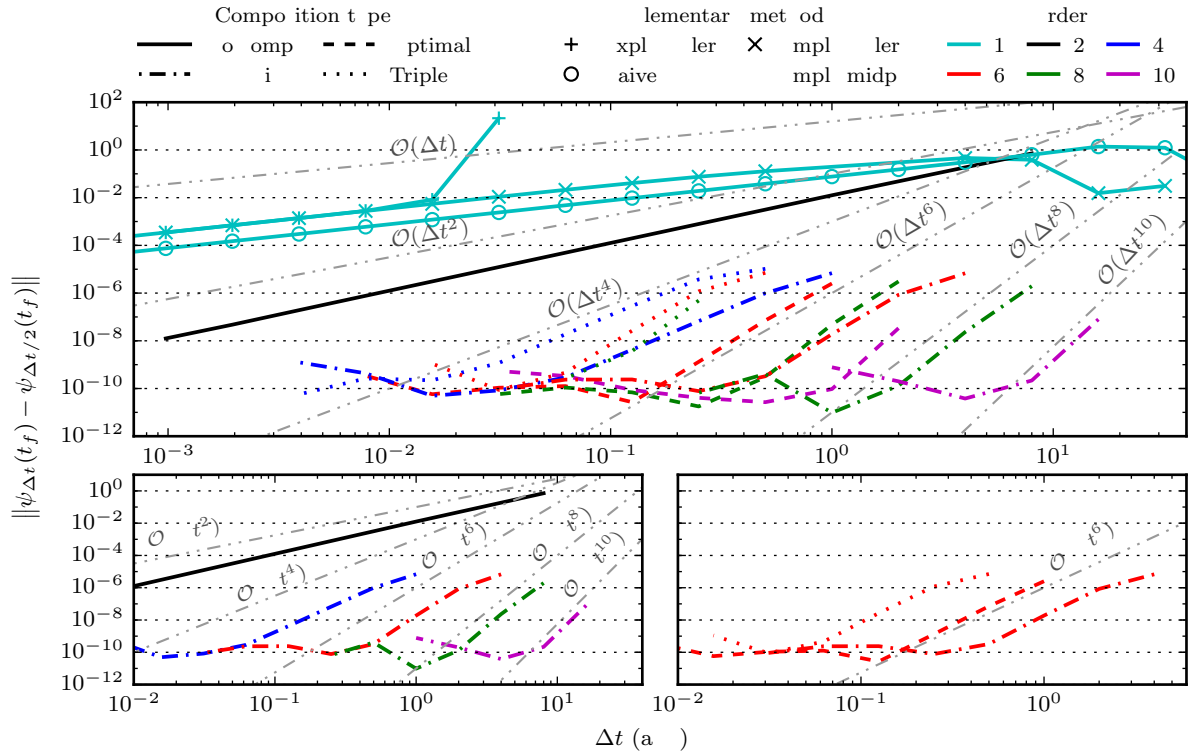


FIG. S3. Same as Fig. S1, but for energy control without nonadiabatic couplings.

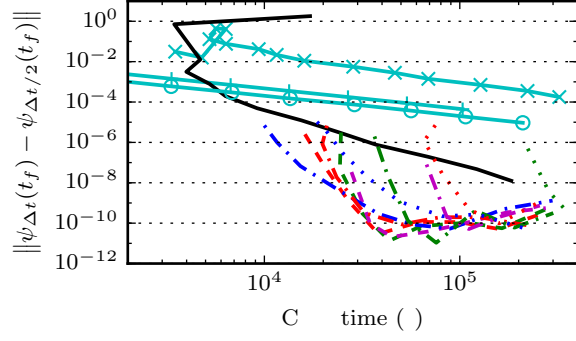


FIG. S4. Efficiency of the integrators used for the local population control of retinal in the absence of nonadiabatic couplings. Efficiency is measured by plotting the convergence error as a function of the computational (CPU) cost. Simulations were performed using both Euler methods, the naïve TVT split-operator algorithm as well as the implicit midpoint method and its symmetric compositions.

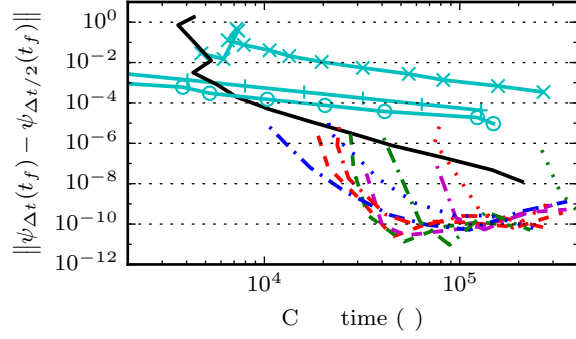


FIG. S5. Same as Fig. S4, but for energy control with nonadiabatic couplings.

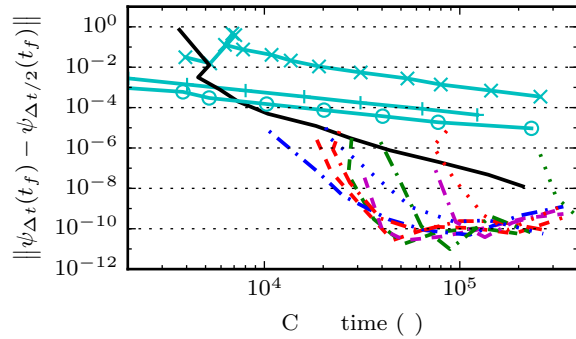


FIG. S6. Same as Fig. S4, but for energy control without nonadiabatic couplings.

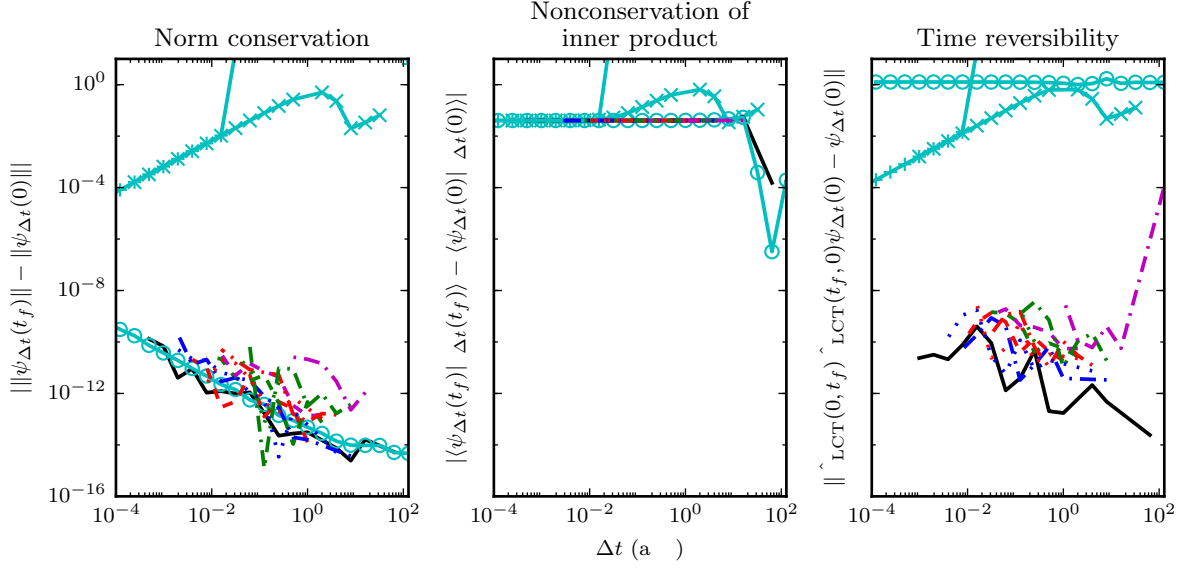


FIG. S7. Conservation of norm (left), inner product (center) and time reversibility (right) of the integrators for the local control of population in the absence of nonadiabatic couplings. $\theta(0)$ is $\psi(0)$ displaced along the reaction coordinate, i.e., a Gaussian wavepacket with parameters $q_0 = (0.1, 0)$, $p_0 = (0, 0)$, and $\sigma_0 = (0.128, 0)$ a.u. Time reversibility is measured as the distance between the initial state ψ_0 and a state $\hat{U}_{\text{LCT}}(0, t_f)\hat{U}_{\text{LCT}}(t_f, 0)\psi(0)$, obtained by propagating $\psi(0)$ first forward in time for time t_f and then backward in time for time t_f .

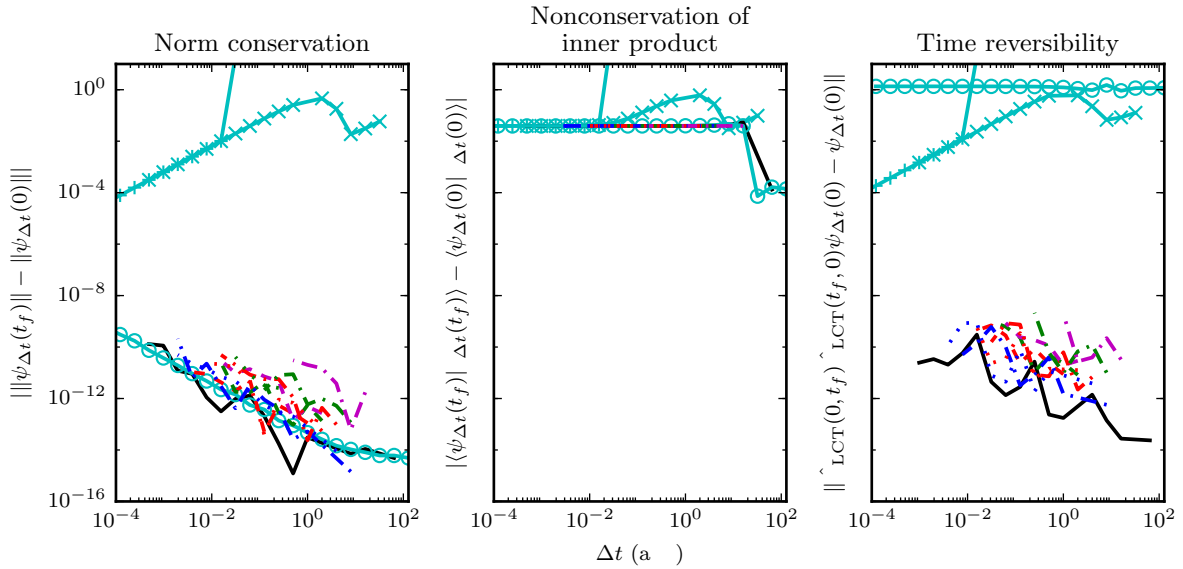


FIG. S8. Same as Fig S7, but for energy control with nonadiabatic couplings.

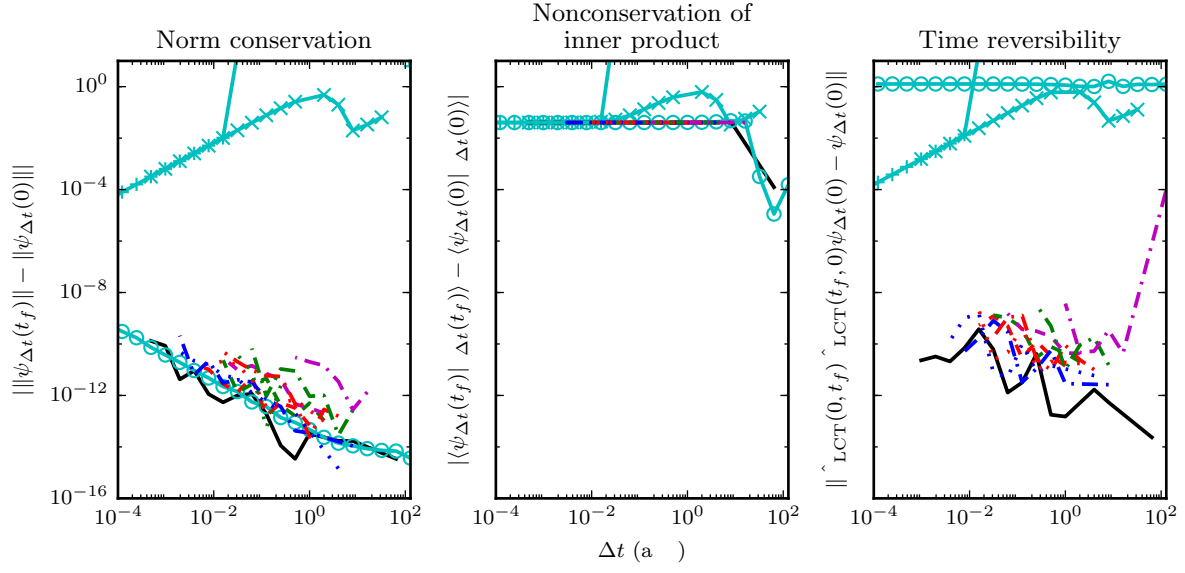


FIG. S9. Same as Fig S7, but for energy control without nonadiabatic couplings.